Journal of Alloys and Compounds 800 (2019) 314–319

Contents lists available at ScienceDirect

Journal of Alloys and Compounds

journal homepage: http://www.elsevier.com/locate/jalcom

Accurate measurement of glass transition temperature of $Cu_{47.5}Zr_{47.5}Al_5$ and $Zr_{41.2}Ti_{13.8}Cu_{12.5}Ni_{10}Be_{22.5}$ using step-scan modulated differential scanning calorimeter

Parijat P. Jana, Jayanta Das*

Department of Metallurgical and Materials Engineering, Indian Institute of Technology Kharagpur, 721302, India

ARTICLE INFO

Article history:
Received 11 October 2018
Received in revised form
20 April 2019
Accepted 4 June 2019
Available online 5 June 2019

Keywords:
Bulk metallic glass
Glass transition
Enthalpy
Transmission electron microscopy
Step-scan modulated differential scanning calorimeter

ABSTRACT

The onset of the glass transition (T_g^{onset}) and crystallization (T_x) temperatures of $Cu_{47.5}Zr_{47.5}Al_5$ and $Zr_{41.2}Ti_{13.8}Cu_{12.5}Ni_{10}Be_{22.5}$ (Vitreloy 1) plates were investigated using conventional differential scanning calorimeter (DSC) and step-scan modulated differential scanning calorimeter (MDSC). A large scatter of the T_g^{onset} values with error of ±6.9 K for $Cu_{47.5}Zr_{47.5}Al_5$ and ±8.0 K for Vitreloy 1 have been observed, at a heating rate of 20 K/min using conventional DSC. Such variation is linked with the variation of the enthalpy change of the respective metallic glass up to different extent prior to the glass transition. Our investigation shows that the T_g^{onset} values can be accurately estimated from the reversible heat flow curve with an error of ±0.6 K using step-scan MDSC analysis, which eliminates the effect of enthalpy change near to the glass transition.

1. Introduction

The mechanical and physical properties of the metallic glasses (MGs) as well as bulk metallic glasses (BMGs) depend on the adopted fabrication process, processing parameters such as, cooling rates, melt temperature etc., and thermal history [1–4]. Therefore, the glass transition temperature (T_g) is one of the most crucial parameter for characterizing and understanding the glassy structure. The T_g is defined kinetically as the temperature at which the viscosity of the transforming liquid reaches to a maximum value of 10^{12} Pa s at a cooling rate of 0.33 K/s [5]. On the other hand, the thermodynamic definition of T_g as derived from the differential scanning calorimeter (DSC), is the temperature at which the measured heat capacity (C_p) at a constant heating rate abruptly starts to increase [6]. Therefore, the T_g is strongly influenced by the composition of the atomic cluster and its configuration namely the short range order (SRO) of the metallic glasses, which significantly affect on the thermo-analytical properties of the MGs/BMGs [7]. Hence, the T_g and the crystallization temperature (T_x) of many glass-forming alloys have been extensively studied using not only DSC but also using differential thermal analyzer (DTA), dynamic mechanical analyzer (DMA) [8,9]. However, the characterization of T_g and T_x using DSC is common due to the simple experimental parameters, high sensitivity of the instrument and acquired data with high resolution [10].

The applications of Zr-based BMGs as compared to the crystalline steel and Ti-alloys are of great scientific importance due to the high Young's modulus of the Zr-based BMGs (~96 GPa), and large elastic strain-to-failure limit ($\varepsilon_{el} \approx 2\%$) as compared to steel ($\varepsilon_{el} \approx 0.5\%$) and Ti- alloys ($\varepsilon_{el} \approx 0.5\%$). These BMGs posses high tensile yield strength (~1.9 GPa) as compared to the high strength steel (1 GPa) and Ti-alloys (~0.73 GPa). The Zr based BMGs show high specific strength of 0.32 GPa g^{-1} cm^{-3}, which is much higher than that of steels (<0.21 GPa g^{-1} cm^{-3}) and Ti- alloys (<0.31 GPa g^{-1} cm^{-3}) [11]. Apart from these engineering properties Zr-based BMGs show greater resistance to plastic deformation due to high fracture toughness, low damping, near net shape fabrication due to low shrinkage, and high corrosion resistance. Therefore, the Zr-based BMGs find application as golf club heads, tennis racket frames, casing for electronic devices, pressure sensors, bio-medical application for knee replacement as well as many devices and surgical equipment, etc. [12].

Step-scan MDSC is an extension of the conventional DSC program, which provides information about the reversible and nonreversible characteristics of a thermal event, which can be performed using either power compensated or heat flux DSC [13].

* Corresponding author.
E-mail address: j.das@metal.iitkgp.ac.in (J. Das).

https://doi.org/10.1016/j.jallcom.2019.06.052
0925-8388/

The step-scan MDSC differs from the conventional DSC in the sense that a temperature profile i.e., steps in the temperature during heating or cooling is applied to the sample and to the reference with particular number of repetitions depending on the temperature range of interest is overlaid on the standard linear heating scans. In the case of a step-scan MDSC, the total heat flow signal can be divided into the non-reversing and reversing components. The reversing component can be identified during the heating segment, whereas, the non-reversing component is identified on the isothermal segment [14,15]. The experimental variables during the step-scan MDSC studies are the linear heating rate, step size i.e., temperature jump between two subsequent isothermal holding segments, duration of the isothermal segment, and frequency of the steps. Hence, the heat flow can be represented mathematically using following equation [14].

$$\frac{dQ}{dt} = [\mathrm{Cp}\,(t) + f'(T, t).]\,\beta + f\,(T, t) \quad (1)$$

Where, $\frac{dQ}{dt}$ is the total heat flow from the sample measured in mW, β is the heating rate (K/min), C_p is the sample heat capacity (J/g.K), t = time, T = temperature, $f'(T, t)$ is the thermodynamic heat flow component, and $f(T, t)$ is the kinetically-estimated heat flow. According to the Equation (1), the total heat flow comprises of two components, one of which is heating rate dependent, and the other one depends only on the absolute temperature and time. The heating rate dependent transitions such as heat capacity, glass transition etc., are reversing in nature. On the other hand, the absolute temperature and time dependent transitions, such as relaxation, crystallization, curing, evaporation, and decomposition are non-reversing in the nature [16]. The step-scan MDSC facilitates the separation of the reversing and non-reversing transitions [14]. The raw data obtained from the step-scan MDSC trace can be deconvoluted using Pyris software to obtain the reversing and non-reversing components of the total heat flow. The glass transition phenomenon is reversing in nature and appears on the reversible heat flow curve (RHF). Whereas, crystallization of metallic glass is non-reversing in nature, and appears on the non-reversible heat flow curve (NHF). Moreover, the step-scan MDSC curve can be analysed on the basis of the amplitude value of the heat flow curve (ΔY method) or the area under the heat flow curve (Area method).

In this work, we report the large scatter of the T_g^{onset} value for similarly processed BMGs can be precisely measured by using step-scan MDSC. The conventional DSC studies show a wide range of T_g^{onset} values for similarly processed $Cu_{47.5}Zr_{47.5}Al_5$ and Vitreloy 1 BMGs both in the present study as well as the data reported in the literatures. Our analysis of T_g and T_x using various algorithms during step-scan MDSC studies shows a narrow range of T_g^{onset} values for the studied BMGs.

2. Experimental

Nominal composition of $Cu_{47.5}Zr_{47.5}Al_5$ (*at.%*) was prepared by arc melting of pure Cu, Zr, and Al in Ti-gettered argon atmosphere. The ingot was remelted several times to achieve chemical homogeneity. As-cast plates with dimension $4 \times 2 \times 70\ mm^3$ were prepared by suction casting facility attached to the arc melter. Vitreloy 1 ($Zr_{41.2}Ti_{13.8}Cu_{12.5}Ni_{10}Be_{22.5}$) plates of dimension $6 \times 1.5 \times 20\ mm^3$ were received from Liquid Metal Technologies (Lake forest, California). The structural investigation was performed using a high-resolution x-ray diffractometer (XRD, Philips PANalytical PW3373, Netherlands) with Cu–Kα radiation. An analytical transmission electron microscope (TEM) (Technai G^2 20, USA) operated at 200 kV, was used for microstructural characterization. Samples for TEM studies were prepared using precision ion polishing system (Gatan PIPS-691) with liquid N_2 cooling facility. A high-resolution field emission scanning electron microscope (FESEM; SUPRA 40 Carl-Zeiss SMT AG, Oberkochen, Germany) equipped with an energy dispersive x-ray spectrometer (EDS) have been used to analyze the alloy composition at different locations of the large plate to verify the chemical homogeneity along their length and cross-section. The thermo-analytical measurements for both conventional DSC and step-scan MDSC were performed using a Perkin Elmer DSC 8000 differential scanning calorimeter. The DSC was calibrated for baseline heat flow, furnace (i.e. temperature), and enthalpy using Zn and In standard at heating rates of 5 K/min and 20 K/min under the flow of high purity N_2 gas (20 ml/min) in the temperature range of 293 K and 783 K. Step-scan MDSC was performed in the temperature range of 573K and 753K with stepped scan of 1 K at the rate of 5 K/min with 180 repetitions. Plate specimens of ~20–40 mg were cut using a diamond blade cutter, polished on 1200 and 2000 grit SiC paper, and were cleaned using acetone in ultrasonic cleaner in order to remove surface contamination prior to the conventional DSC and step-scan MDSC experiments. The thermogram of an empty aluminium pan was used to establish the baseline curve for conventional DSC and step-scan MDSC measurements. Minimum 2–5 specimens were tested in both conventional DSC and MDSC to obtain the repetitive T_g^{onset} and T_x values.

3. Results and discussion

3.1. Structural characterization

The TEM images of the $Cu_{47.5}Zr_{47.5}Al_5$ and Vitreloy 1 are shown in Fig. 1(a) and (b) respectively. The presence of homogeneous structure is confirmed, as there is no variation in the contrast as observed in the TEM images. The corresponding selected area electron diffraction (SAED) patterns are shown in the inset of the respective samples. The presence of diffused halo in the SAED patterns confirms the structure is fully glassy in both the samples. The XRD patterns of $Cu_{47.5}Zr_{47.5}Al_5$ and Vitreloy 1 are shown in inset of Fig. 1(a) and (b) respectively. The appearance of broad diffraction maximum in both the patterns confirms the characteristic feature of the glassy structure. The reference patterns of cubic B2 CuZr (JCPDS#00-049-1483) and tetragonal $CuZr_2$ (#03-065-2647) in case of $Cu_{47.5}Zr_{47.5}Al_5$, and hexagonal $BeZr_2$ (#00-012-0392) and orthorhombic $Cu_{10}Zr_7$ (#00-042-1187) in case of Vitreloy 1, have been incorporated in the inset of Fig. 1(a and b), respectively. The theoretical reference patterns of the selected compounds were chosen, since these are the products of crystallization of the glassy phase, as reported in the literature [17,18] The above experimental observations are consistent and nano-crystallization or phase separations have not been noticed. The EDS analysis revealed that the bulk glassy specimens contain Cu (47.5 ± 0.4 *at.%*), Zr (47.2 ± 0.5 *at.%*), and Al (5.3 ± 0.1 *at.%*) for $Cu_{47.5}Zr_{47.5}Al_5$ and Zr (44.7 ± 0.4 *at.%*), Ti (11.6 ± 0.1 *at.%*), Ni (10.7 ± 0.1 *at.%*), Cu (10.5 ± 0.3 *at.%*) for $Zr_{41.2}Ti_{13.8}Cu_{12.5}Ni_{10}Be_{22.5}$ assuming the Be content to be 22.5 *at.%*. The error (±) values were obtained from the multiple measurements from different locations across the section and length of the investigated glassy alloys.

3.2. Conventional DSC studies

Fig. 2(a) displays the conventional DSC thermograms of $Cu_{47.5}Zr_{47.5}Al_5$ at heating rates of 5 K/min and 20 K/min. The DSC trace of the samples display a broad endothermic peak followed by the supercooled liquid region (SLR), and a sharp exothermic peak. The endothermic peak arises due to the glass transition event, whereas the exothermic peak is linked with the crystallization of

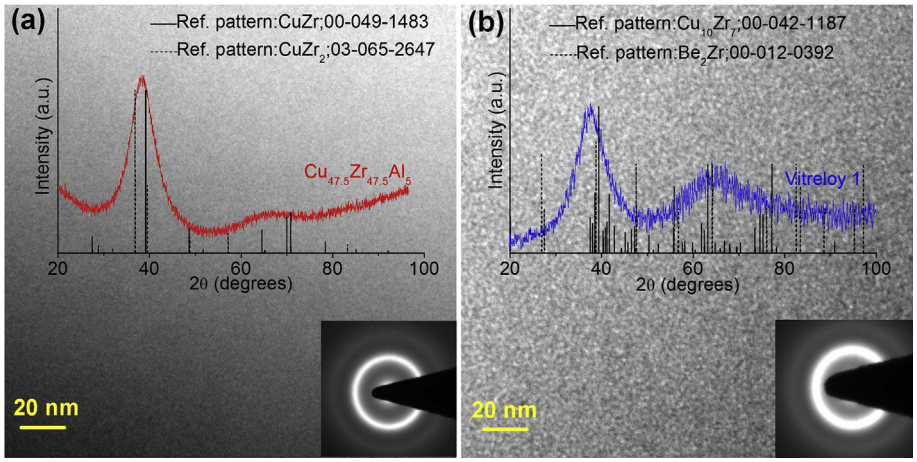

Fig. 1. TEM bright field image of (a) $Cu_{47.5}Zr_{47.5}Al_5$, and (b) Vitreloy-1 showing the glassy structure. The selected area electron diffraction patterns and x-ray diffraction patterns of the corresponding samples are shown in inset.

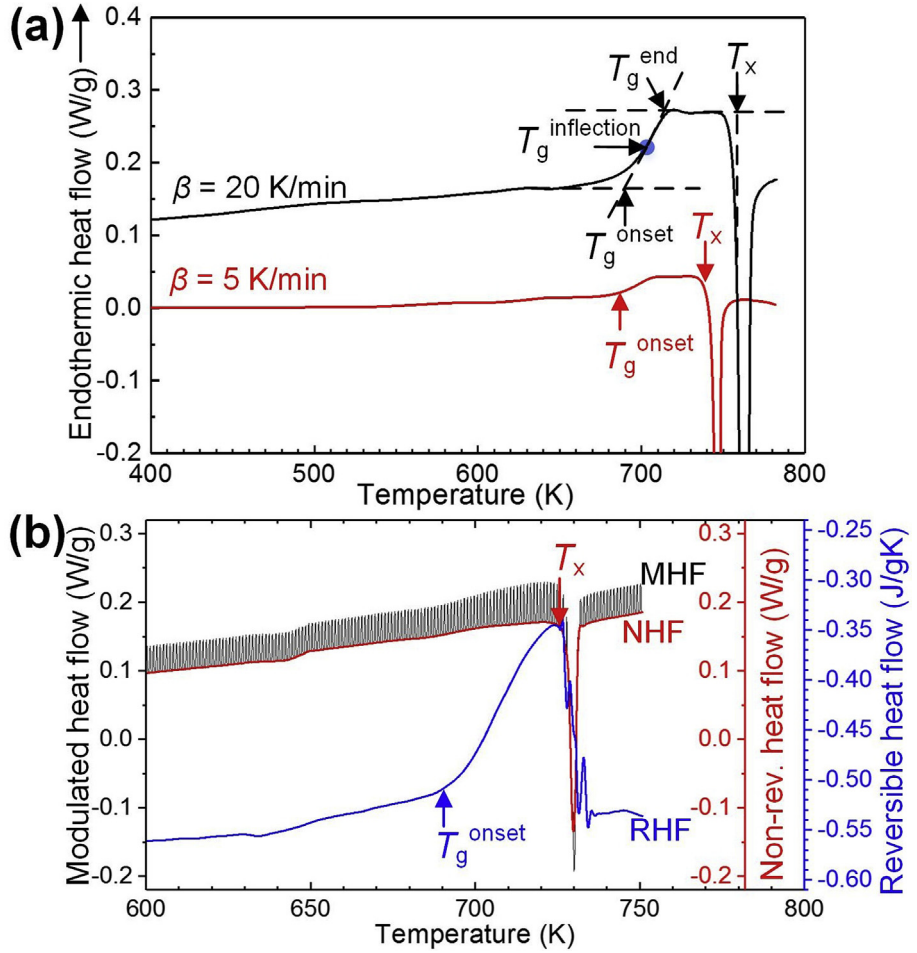

Fig. 2. (a) Conventional DSC plots of $Cu_{47.5}Zr_{47.5}Al_5$ plate at a heating rate of 20 K/min and 5 K/min showing the characteristics temperatures such as T_g^{onset}, $T_g^{inflection}$, T_g^{end}, and T_x. (b) Step-scan MDSC plot of $Cu_{47.5}Zr_{47.5}Al_5$ showing the variation of modulated heat flow (MHF), non-reversible heat flow (NHF), and reversible heat flow (RHF) with temperature.

the supercooled liquid. The inflection of glass transition ($T_g^{inflection}$) is labeled as the point, at which the slope of the endothermic heat flow versus temperature curve starts decreasing. Therefore, the T_g^{onset} is defined as the intersection point of the tangent at the left limit point and the tangent at inflection point. On the other hand, the T_g^{end} is defined as the intersection of the tangents at the right limit point and the tangent at the inflection point. The values of T_g^{onset} and T_x are assessed from the equivalent onset values. The temperatures of T_g^{onset}, $T_g^{inflection}$, T_g^{end}, and T_x are marked by arrows in Fig. 2(a). It has been revealed that the T_g^{onset} value depends on the adopted heating rate during conventional DSC scans. The higher heating rate leads to the higher value of T_g^{onset}, as depicted in Fig. 2

(a) and Table 1. As an example, the T_g^{onset} values (689.4 ± 6.9 K) of $Cu_{47.5}Zr_{47.5}Al_5$ plate at 20 K/min is higher than that of the T_g^{onset} value (684.1 ± 3.7 K) obtained at heating rate of 5 K/min. The variation of T_g^{onset} for $Cu_{47.5}Zr_{47.5}Al_5$ during conventional DSC studies has been estimated to be 689.4 ± 6.9 K and 684.1 ± 3.7 K at heating rate of 20 K/min and 5 K/min, respectively. Such wide variation in the T_g^{onset} value has been also reported in the literature, as summarized in Table 1. The magnified view of the heat flow curves obtained from several conventional DSC traces of the $Cu_{47.5}Zr_{47.5}Al_5$ glassy plate at a heating rate of 20 K/min and 5 K/min are shown in Fig. 3(a) and (b) respectively. The non-identical nature of such heat flow traces indicates the variation in the T_g^{onset} values.

3.3. MDSC studies

The step-scan MDSC scans of $Cu_{47.5}Zr_{47.5}Al_5$ comprising of modulated heat flow (MHF), RHF and NHF curves, are shown in Fig. 2(b). Since the glass transition is an endothermic process, the T_g^{onset} has been estimated from the RHF curve, and the T_x has been estimated from the NHF curve. Fig. 3(c) and (d) show the magnified view of such RHF traces as analysed using ΔY method and area method, respectively, near T_g^{onset} of the $Cu_{47.5}Zr_{47.5}Al_5$, which appear to be identical and superimpose on each other. The T_g^{onset} and T_x values as obtained from the RHF and NHF traces of the step-scan MDSC (ΔY method) of the plate lie in the range of 691.3 ± 0.6 K, and 728.4 ± 0.8 K, respectively.

3.4. Precise estimation of T_g^{onset}

A large number of literature [19–40] have been surveyed to understand the wide variation of the measured T_g^{onset} values in $Cu_{47.5}Zr_{47.5}Al_5$ and Vitreloy 1, which are shown in Table 1. Earlier, the variation of such T_g^{onset} values has been correlated with the different extent of enthalpy change prior to the glass transition event. The change of the exothermic enthalpy (ΔH) near the glass transition event overshadows the endothermic glass transition event. Fig. 4 shows the measured difference in ΔH values with normalized temperature (T/T_g^{onset}) in several DSC traces of $Cu_{47.5}Zr_{47.5}Al_5$ at a heating rate of 20 K/min. The variation of enthalpy (H) with temperature of a glassy specimen during the 1st heating up to 783 K, and the same as acquired during the 2nd heating cycle of the completely crystallized sample, are shown in the inset of Fig. 4. It is evident that the enthalpy of glassy specimen increases rapidly than that of crystalline state at around the glass transition event. Such observation points that the glass phase has higher C_p than that of a crystal [5,41]. Hence, the ΔH value of the $Cu_{47.5}Zr_{47.5}Al_5$ has been estimated by subtracting the enthalpy of the completely crystallize sample from its glassy state.

It is interesting to notice that the increase of ΔH with temperature for the same glassy specimen exhibit large differences and does not superimpose on each other. Such variation of ΔH leads to the erroneous or wide range of the T_g^{onset} values of the studied glasses. However, it is expected that T_g^{onset} values should be very close for different samples collected from the same glassy specimens using same instrument at similar calibration condition at a given heating rate. The results obtained using the conventional DSC for different samples collected from the $Cu_{47.5}Zr_{47.5}Al_5$ glassy plates at 5 K/min and 20 K/min show a large scatter data, as depicted in Fig. 5(a). Moreover, such variation in the T_g^{onset} values were also reported in the literature, as summarized in Table 1. Similarly, Fig. 5(b) shows the variation of T_g^{onset} and T_x values of Vitreloy 1 as obtained in the present study along with the data available in the literature [22–40]. The dotted lines in Fig. 5(a) and (b) represent the data obtained in both the present study and literature data

Table 1
The onset of glass transition temperature (T_g^{onset}), crystallization temperature (T_x), and width of supercooled liquid region (ΔT_x) of $Cu_{47.5}Zr_{47.5}Al_5$ and vitreloy 1 plate (plate thickness t, rod diameter ⌀) estimated using Conventional DSC at heating rate in the range of 5–200 K/min, and step-scan MDSC. The values in (±) are the standard deviation of the measurements.

Sample	β (K/min)	T_g^{onset} (K)	T_x (K)	ΔT_x (K)	Reference
$Cu_{47.5}Zr_{47.5}Al_5$ (t = 2 mm)	5	684.1 ± 3.7	744.9 ± 0.7	60.8 ± 4.1	This work
	20	689.4 ± 6.9	761.8 ± 0.6	72.5 ± 6.5	
	MDSC (ΔY)	691.3 ± 0.6	728.4 ± 0.8	37.0 ± 0.7	
	MDSC (Area)	690.2 ± 0.9	728.5 ± 0.9	38.3 ± 0.3	
Vitreloy 1 (t = 1.5 mm)	20	609.8 ± 8.0	752.5 ± 0.1	142.7 ± 7.9	
	MDSC (ΔY)	626.3	704.1	77.8	
	MDSC (Area)	625.0	704.2	79.2	
$Cu_{47.5}Zr_{47.5}Al_5$ (t = 1.5 mm)	40	706.0	769.0	63.0	[19]
$Cu_{47.5}Zr_{47.5}Al_5$ (⌀ = 2 mm)	40	698.0	772.0	74.0	[20]
$Cu_{47.5}Zr_{47.5}Al_5$ (⌀ = 2 mm)	40	695.0	761.0	66.0	[21]
Vitreloy 1	5	611.0	688.0	77.0	[22]
Vitreloy 1	10	615.0	700.0	85.0	[22]
Vitreloy 1 (⌀ = 3 mm)	10	614.3	695.6	81.3	[23]
Vitreloy 1 (t = 3 mm)	10	625.0	700.0	75.0	[24]
Vitreloy 1 (t = 2 mm)	10	615.0	700.0	85.0	[25]
Vitreloy 1(t = 3.3 mm)	10	636.0	699.0	63.0	[26]
Vitreloy 1	20	619.0	713.0	94.0	[22]
Vitreloy 1	20	623.0	705.0	82.0	[27]
Vitreloy 1 (⌀ >20 mm)	20	623.0	712.0	89.0	[28]
Vitreloy 1	20	640.6	700.1	59.5	[29]
Vitreloy 1 (⌀ = 12.6 mm)	20	623.0	705.0	82.0	[30]
Vitreloy 1 (⌀ = 2 mm)	20	625.0	692.0	67.0	[31]
Vitreloy 1 (⌀ = 12 mm)	20	619.0	709.0	90.0	[32]
Vitreloy 1 (⌀ = 2.5 mm)	20	643.0	713.0	70.0	[33]
Vitreloy 1 (⌀ = 2 mm)	20	619.5	692.0	72.5	[34]
Vitreloy 1 (t = 1.1 mm)	20	635.0	707.8	72.8	[35]
Vitreloy 1 (t = 3 mm)	20	614.0	698.0	84.0	[36]
Vitreloy 1 (t = 4 mm)	20	641.0	698.0	57.0	[37]
Vitreloy 1 (⌀ = 2 mm)	40	638.8	715.6	76.8	[38]
Vitreloy 1 (⌀ = 10 mm)	40	637.0	733.0	96.0	[39]
Vitreloy 1 (t = 7 mm)	40	633.0	723.0	90.0	[40]
Vitreloy 1 (⌀ = 12.6 mm)	200	645.2	763.3	118.1	[30]

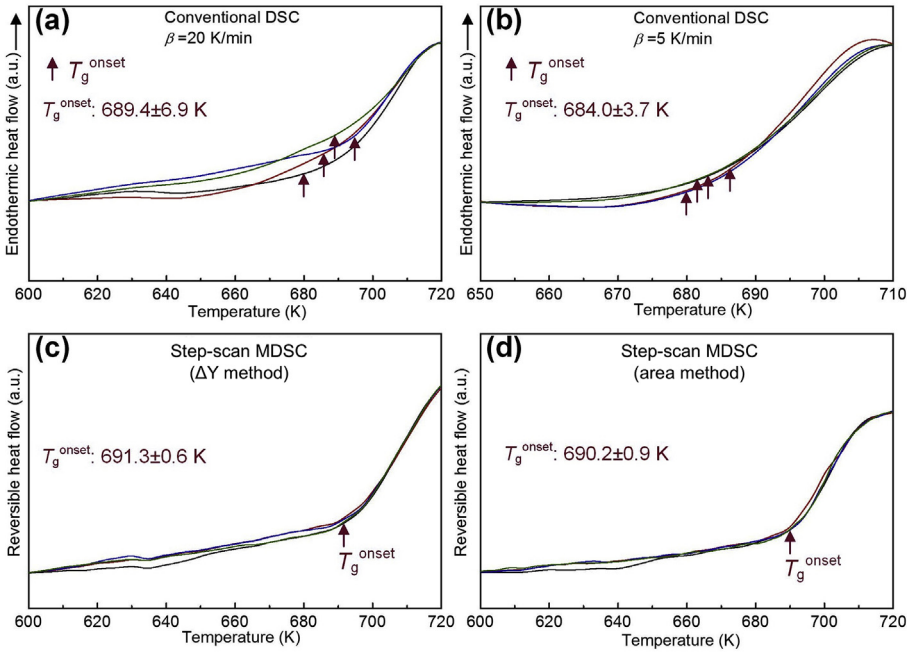

Fig. 3. The magnified view of the normalized heat flow of different DSC traces of $Cu_{47.5}Zr_{47.5}Al_5$ plate at a heating rate of (a) 20 K/min and (b) 5 K/min showing the variation in T_g^{onset}. The enlarged view of RHF traces of $Cu_{47.5}Zr_{47.5}Al_5$ as obtained from ΔY algorithm and area method for accurate measurement of T_g^{onset}.

point at specific heating rate and are used for eye guideline. It is understood that small variation of T_g^{onset} of a given glass as reported by different authors may arise due to the calibration error, slight composition fluctuation in differently prepared samples and the sensitivity of the temperature sensors. Nevertheless, we must consider the effect of the non-reversible enthalpy relaxation prior and during the glass transition event, which lead to the erroneous T_g^{onset} values. Whereas, the RHF curve of step-scan MDSC method exclusively nullify the effect of relaxation prior and during glass transition event. Hence, the T_g^{onset} values can be precisely estimated using the RHF curve of the step-scan MDSC.

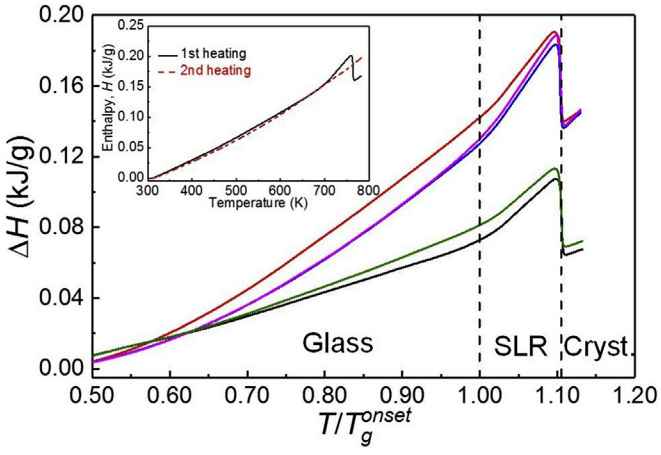

Fig. 4. The measured difference in the enthalpy values between the glass and the crystalline state as a function of normalized temperature (T/T_g^{onset}) in several samples of $Cu_{47.5}Zr_{47.5}Al_5$ using conventional DSC thermograms at heating rate of 20 K/min show a wide variation of the enthalpy relaxation in different samples prior to glass transition. The inset shows the variation of the enthalpy with temperature during 1st heating (glassy) and 2nd heating (crystalline) of $Cu_{47.5}Zr_{47.5}Al_5$.

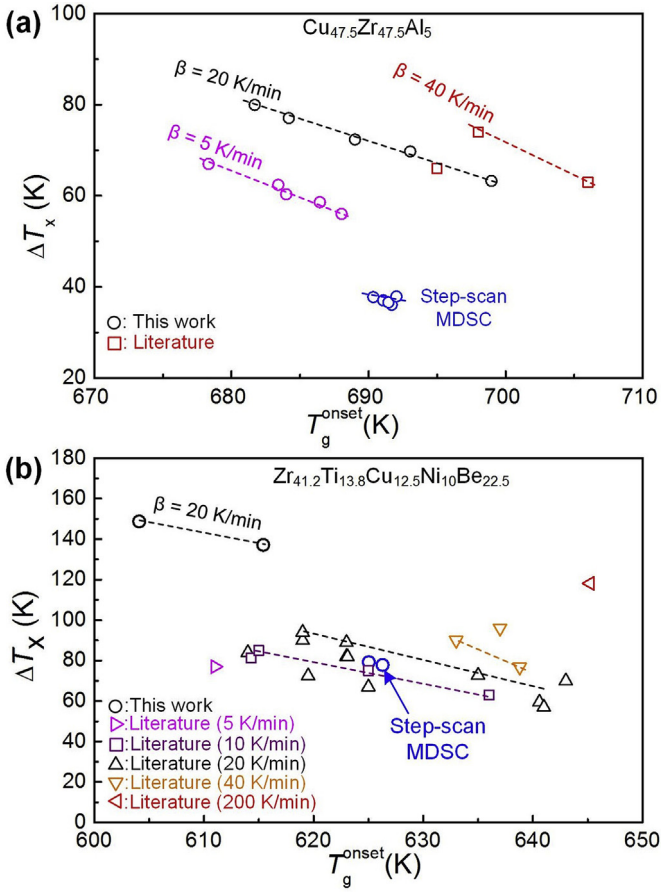

Fig. 5. A wide scatter of T_g^{onset} in (a) $Cu_{47.5}Zr_{47.5}Al_5$ and (b) $Zr_{41.2}Ti_{13.8}Cu_{12.5}Ni_{10}Be_{22.5}$ as measured at heating rates in the range of 5–200 K/min in the present study as well as data reported in the literature using conventional DSC. The T_g^{onset} can be precisely measured using step-scan MDSC.

4. Conclusions

The step-scan MDSC has been adopted to study the glass transition of $Cu_{47.5}Zr_{47.5}Al_5$ and Vitreloy 1. The results have been compared with the conventional DSC studies along with the data previously reported in the literature. A wide range of T_g^{onset} has been observed for similarly processed glassy specimens using conventional DSC. The different extent of enthalpy relaxation prior to glass transition event leads to the erroneous measurement of T_g^{onset} in conventional DSC. Whereas, the T_g^{onset} has been accurately measured for $Cu_{47.5}Zr_{47.5}Al_5$ plate (T_g^{onset}: 691.3 ± 0.6 K) from the C_p change in the RHF curve using step-scan MDSC, which effectively reduces the effect of enthalpy relaxation prior and during the glass transition event.

Acknowledgements

The authors thank M. Das, S. Mandal and S. Maity and for technical assistance. The financial supports provided by SRIC IIT Kharagpur through SGIRG and SGBSI schemes are greatly acknowledged.

References

[1] A. Inoue, High strength bulk amorphous alloys with low critical cooling rates, Mater. Trans., JIM 36 (1995) 866–875.
[2] W.H. Wang, Correlations between elastic moduli and properties in bulk metallic glasses, J. Appl. Phys. 99 (2006) 093506.
[3] B. Yang, C.T. Liu, T.G. Nieh, Unified equation for the strength of bulk metallic glasses, Appl. Phys. Lett. 63 (1993) 221911.
[4] R.T. Qu, Z.Q. Liu, R.F. Wang, Z.F. Zhang, Yield strength and yield strain of metallic glasses and their correlations with glass transition temperature, J. Alloy. Comp. 637 (2015) 44–54.
[5] A.L. Greer, Y.H. Sun, Stored energy in metallic glasses due to strains within the elastic limit, Philos. Mag. 96 (2016) 1643–1663.
[6] M.I. Ojovan, Ordering and structural changes at the glass–liquid transition, J. Non-Cryst. Solids 382 (2013) 79–86.
[7] J. Saida, R. Yamada, M. Wakeda, S. Ogata, Thermal rejuvenation in metallic glasses, Sci. Technol. Adv. Mater. 18 (2017) 152–162.
[8] O. Haruyama, Y. Nakayama, R. Wada, H. Tokunaga, J. Okada, T. Ishikawa, Y. Yokoyama, Volume and enthalpy relaxation in $Zr_{55}Cu_{30}Ni_5Al_{10}$ bulk metallic glass, Acta Mater. 58 (2010) 1829–1836.
[9] J.C. Qiao, J. Cong, Q. Wang, J.M. Pelletier, Y. Yao, Effects of iron addition on the dynamic mechanical relaxation of $Zr_{55}Cu_{30}Ni_5Al_{10}$ bulk metallic glasses, J. Alloy. Comp. 749 (2018) 262–267.
[10] P.P. Jana, J. Das, Precise estimation of glass transition and crystallization temperatures of $Zr_{55}Cu_{30}Ni_5Al_{10}$ metallic glass using step-scan modulated temperature differential scanning calorimeter, Thermochim. Acta 550 (2018) 18–22.
[11] M. Telford, The case for bulk metallic glasses, Mater. Today 7 (2004) 37–43.
[12] A. Inoue, Bulk glassy alloys: historical development and current research, Engineering 1 (2015) 185–191.
[13] A. Boller, C. Schick, B. Wunderlich, Modulated differential scanning calorimetry in the glass transition region, Thermochim. Acta 266 (1995) 97–111.
[14] K. Pielichowski, K. Flejtuch, J. Pielichowski, Step-scan alternating DSC study of melting and crystallisation in poly (ethylene oxide), Polymer 45 (2004) 1235–1242.
[15] P.S. Gill, S.R. Sauerbrunn, M. Reading, Modulated differential scanning calorimetry, J. Therm. Anal. 40 (1993) 931–939.
[16] M. Sandor, N.A. Bailey, E. Mathiowitz, Characterization of polyanhydride microsphere degradation by DSC, Polymer 43 (2002) 279–288.
[17] S. Pauly, G. Liu, G. Wang, U. Kühn, N. Mattern, J. Eckert, Microstructural heterogeneities governing the deformation of $Cu_{47.5}Zr_{47.5}Al_5$ bulk metallic glass composites, Acta Mater. 57 (2009) 5445–5453.
[18] S.J. Chung, K.T. Hong, M.R. Ok, J.K. Yoon, G.H. Kim, Y.S. Ji, B.S. Seong, K.S. Lee, Analysis of the crystallization of $Zr_{41}Ti_{14}Cu_{12.5}Ni_{10}Be_{22.5}$ bulk metallic glass using electrical resistivity measurement, Scripta Mater. 53 (2005) 223–228.
[19] K.K. Song, S. Pauly, Y. Zhang, S. Scudino, P. Gargarella, K.B. Surreddi, U. Kühn, J. Eckert, Significant tensile ductility induced by cold rolling in $Cu_{47.5}Zr_{47.5}Al_5$ bulk metallic glass, Intermetallics 19 (2011) 1394–1398.
[20] J. Eckert, J. Das, K.B. Kim, F. Baier, M.B. Tang, W.H. Wang, Z.F. Zhang, High strength ductile Cu-base metallic glass, Intermetallics 14 (2006) 876–881.
[21] R. Limbach, K. Kosiba, S. Pauly, U. Kühn, L. Wondraczek, Serrated flow of CuZr-based bulk metallic glasses probed by nanoindentation: role of the activation barrier, size and distribution of shear transformation zones, J. Non-Cryst. Solids 459 (2017) 130–141.
[22] M.-R. Ok, J.-Y. Suh, S.J. Chung, Y.S. Ji, K.T. Hong, Micro-forming and surface evaluation of $Zr_{41}Ti_{14}Cu_{12.5}Ni_{10}Be_{22.5}$ bulk metallic glass, Mater. Sci. Eng. A 454–455 (2007) 14–18.
[23] Q. Wang, D.K. Wang, T. Fu, J.J. Blandin, J.M. Pelletier, Y.D. Dong, High temperature homogeneous plastic flow behavior of a Zr based bulk metallic glass matrix composite, J. Alloy. Comp. 495 (2010) 50–54.
[24] P. Murali, U. Ramamurty, Embrittlement of a bulk metallic glass due to sub-T_g annealing, Acta Mater. 53 (2005) 1467–1478.
[25] S.J. Chung, K.T. Hong, M.-R. Ok, J.-K. Yoon, G.-H. Kim, Y.S. Ji, B.S. Seong, K.S. Lee, Analysis of the crystallization of $Zr_{41}Ti_{14}Cu_{12.5}Ni_{10}Be_{22.5}$ bulk metallic glass using electrical resistivity measurement, Scripta Mater. 53 (2005) 223–228.
[26] J.M. Pelletier, B.V. de Moortèle, Phase separation and crystallization in the $Zr_{41.2}$–$Ti_{13.8}$–$Cu_{12.5}$–Ni_{10}–$Be_{22.5}$ bulk metallic glass determined by physical measurements and electron microscopy, J. Non-Cryst. Solids 325 (2003) 133–141.
[27] J. Lu, G. Ravichandran, W.L. Johnson, Deformation behavior of the $Zr_{41.2}Ti_{13.8}Cu_{12.5}Ni_{10}Be_{22.5}$ bulk metallic glass over a wide range of strain-rates and temperatures, Acta Mater. 51 (2003) 3429–3443.
[28] G. Duan, A. Wiest, M.L. Lind, A. Kahl, W.L. Johnson, Lightweight Ti-based bulk metallic glasses excluding late transition metals, Scripta Mater. 58 (2008) 465–468.
[29] M.Q. Jiang, M. Naderi, Y.J. Wang, M. Peterlechner, X.F. Liu, F. Zeng, F. Jiang, L.H. Dai, G. Wilde, Thermal expansion accompanying the glass-liquid transition and crystallization, AIP Adv. 5 (2015) 127133.
[30] A. Peker, W.L. Johnson, A highly processable metallic glass: $Zr_{41.2}Ti_{13.8}Cu_{12.5}$-$Ni_{10}Be_{22.5}$, Appl. Phys. Lett. 63 (1993) 2342–2343.
[31] E. Fleury, S.M. Lee, H.S. Ahn, W.T. Kim, D.H. Kim, Tribological properties of bulk metallic glasses, Mater. Sci. Eng. A 375–377 (2004) 276–279.
[32] C.H. Wong, C.H. Shek, Friction welding of $Zr_{41}Ti_{14}Cu_{12.5}Ni_{10}Be_{22.5}$ bulk metallic glass, Scripta Mater. 49 (2003) 393–397.
[33] D. Suh, P.A. Kumar, R.H. Dauskardt, The effects of hydrogen on viscoelastic relaxation in Zr–Ti–Ni–Cu–Be bulk metallic glasses: implications for hydrogen embrittlement, Acta Mater. 50 (2002) 537–551.
[34] X. Liu, M.D. Demetriou, G. Kaltenboeck, J.P. Schramm, G.R. Garrett, W.L. Johnson, Description of millisecond Ohmic heating and forming of metallic glasses, Acta Mater. 61 (2013) 3060–3067.
[35] T.A. Waniuk, R. Busch, A. Masuhr, W.L. Johnson, Equilibrium viscosity of the $Zr_{41.2}Ti_{13.8}Cu_{12.5}Ni_{10}Be_{22.5}$ bulk metallic glass-forming liquid and viscous flow during relaxation, phase separation, and primary crystallization, Acta Matell. 46 (1998) 5229–5236.
[36] M.E. Kassner, K. Smith, V. Eliasson, Creep in amorphous metals, J. Mater. Res. Technol. 4 (2015) 100–107.
[37] J.S. Park, H.K. Lim, J.-H. Kim, H.J. Chang, W.T. Kim, D.H. Kim, E. Fleury, In situ crystallization and enhanced mechanical properties of $Zr_{41.2}Ti_{13.8}Cu_{12.5}$-$Ni_{10}Be_{22.5}$ alloy by cold rolling, J. Non-Cryst. Solids 351 (2005) 2142–2146.
[38] P. Yu, H.Y. Bai, J.G. Zhao, C.Q. Jin, W.H. Wang, Pressure effects on mechanical properties of bulk metallic glass, Appl. Phys. Lett. 90 (2007), 051906.
[39] H. Huang, J. Yan, On the surface characteristics of a Zr-based bulk metallic glass processed by microelectrical discharge machining, App. Surf. Sci. 355 (2015) 1306–1315.
[40] A.V. Sergueeva, N. Mara, A.K. Mukherjee, Mechanical response of Zr-based metallic glass, J. Non-Cryst. Solids 317 (2003) 169–175.
[41] S.C. Glade, R. Busch, D.S. Lee, W.L. Johnson, R.K. Wunderlich, H.J. Fecht, Thermodynamics of $Cu_{47}Ti_{34}Zr_{11}Ni_8$, $Zr_{52.5}Cu_{17.9}Ni_{14.6}Al_{10}Ti_5$ and $Zr_{57}Cu_{15.4}$-$Ni_{12.6}Al_{10}Nb_5$ bulk metallic glass forming alloys, J. Appl. Phys. 87 (2000) 7242–7248.